Palaeontologia Electronica
palaeo-electronica.org

Reconstruction of the musculoskeletal system in an extinct lion

Andrew R Cuff, Anjali Goswami, and John R. Hutchinson

ABSTRACT

Panthera atrox is an extinct lion from the Pleistocene of North America that is one of the largest felids that has ever existed. Previous reconstructions have always relied on composite specimens, and there are no known specimens that preserve soft tissues. Here we present a reconstruction of the most complete *P. atrox* specimen discovered to date, from which we calculate key biological parameters including body mass. Using previously published scaling equations we estimate the size of the musculature of the limbs and vertebral column. Muscles from a modern lion were scaled to the expected sizes and placed on the skeleton. The body and the limbs were digitally reconstructed (using a convex hulling method) from the skeleton before this method was repeated with the muscled limb segments. Our results from repeating this approach for a modern lion show that the combined muscle and bone convex hull reconstructions are the most accurate for reproducing the limb dimensions, including centres of mass, of large felids. From the reconstructions it is also possible to estimate the body composition of *P. atrox*, which allows for the most complete soft tissue reconstruction of this extinct species, including biomechanical properties of the limbs.

Andrew R Cuff. Department of Genetics, Evolution and Environment, University College London, Darwin Building, Gower Street, London, WC1E 6BT, United Kingdom; Structure and Motion Lab, Department of Comparative Biomedical Sciences, The Royal Veterinary College, Hawkshead Lane, North Mymms, Hatfield, Herts, AL9 7TA, United Kingdom. acuff@rvc.ac.uk
Anjali Goswami. Department of Genetics, Evolution and Environment, University College London, Darwin Building, Gower Street, London, WC1E 6BT, United Kingdom. a.goswami@ucl.ac.uk
John R. Hutchinson. Structure and Motion Lab, Department of Comparative Biomedical Sciences, The Royal Veterinary College, Hawkshead Lane, North Mymms, Hatfield, Herts, AL9 7TA, United Kingdom; Department of Genetics, Evolution and Environment, University College London, Darwin Building, Gower Street, London, WC1E 6BT, United Kingdom. jhutchinson@rvc.ac.uk

Keywords: fossil reconstruction; muscles; Felidae; *Panthera atrox*; scaling

Submission: 3 June 2016 Acceptance: 1 May 2017

Cuff, Andrew R., Goswami, Anjali, and Hutchinson, John R. 2017. Reconstruction of the musculoskeletal system in an extinct lion. *Palaeontologia Electronica* 20.2.23A: 1-25
palaeo-electronica.org/content/2017/1857-reconstructing-a-fossil-lion

INTRODUCTION

Soft tissues seldom are preserved during the fossilisation process, and, as such, most reconstructions of fossil taxa must be based, in terms of direct evidence, solely upon the skeletal remains. Those remains can be incredibly useful for reconstructing myology as the muscles often leave scars on the bone where they attach (Witmer, 1995). However, not all muscles are sufficiently large to produce muscle scars, or they may share similar or obscure attachment sites that can make them difficult to locate (Bryant and Seymour, 1990). For these ambiguous muscles, it may be possible to reconstruct soft tissues based on their presence/absence and qualitative or relative positions using the extant phylogenetic bracket (EPB) approach (Witmer, 1995). However, this method cannot calculate how large the muscles may be in the extinct species, or accurately estimate other quantifiable aspects of their anatomy. Various methods may be used to constrain muscle sizes, e.g., using the bony margins of their attachments and their pathways relative to other muscles (Hutchinson et al., 2011; Allen et al., 2013; Lautenschlager 2013; Persons IV et al., 2013; Cuff and Rayfield, 2015). However, it becomes more difficult to estimate muscle boundaries when there is no outer limit on the size of the muscles. Using convex hulls (e.g., Basu et al., 2016) or non-uniform rational b-splines (NURBs) (e.g., Bates et al., 2009) it is possible to estimate muscle volumes, but doing so incurs additional uncertainties from assumptions of the volume reconstruction methods. Thus advances in the area of soft tissue reconstruction, especially quantitative methods that can also address uncertainties, are important.

Panthera atrox (Leidy, 1853), the "American lion," was a large felid that lived in North America during the Pleistocene epoch before going extinct at the end of the last ice age, approximately 11ka. *Panthera atrox* was derived from a Beringian population of *P. spelaea* (cave lion) evolving around 337ka (Barnett et al., 2009), with both species splitting from *P. leo* around 1.89Ma (Barnett et al., 2016). *P. atrox* has gained much attention over the last few decades due to the size of some of the specimens, with body mass estimates from the largest specimens ranging from 350 kg–420 kg (Sorkin, 2008), making the species one of the largest felids ever to have lived. However, due to the limited number of articulated or associated specimens, reconstructions have been based on composite specimens.

Here we outline a simple method for virtually reconstructing entire postcrania from CT scans using a well-preserved *Panthera atrox* specimen. Using muscle scaling equations from Cuff et al. (2016a, 2016b) for extant felids, we were able to estimate muscle and tendon masses and lengths for the individual. Digital representations of actual muscles from an Asian lion were then scaled so that the dimensions of the locomotor musculature of the limbs and vertebral column were reconstructed and could be placed in the appropriate positions as determined from dissections of living relatives via the EPB method. We also check how well our muscled restorations match the results of different convex hull methods applied to regions of the body.

METHODS

Page Museum specimen LACMP23-555 is a remarkably well-preserved skull and postcranial skeleton of *Panthera atrox* from the La Brea Tar Pits (Project 23-1), dating to approximately 35 ka (Fuller et al., 2014). The remains consist of a complete skull, complete limbs (minus manus and pes), girdles (although scapulae and pelvis are damaged), and a relatively complete vertebral column up to the caudal vertebrae (minus thoracic vertebrate T1, T5, T7, and T10). All of the bones were microCT scanned at The Aerospace Corporation (El Segundo, California, USA), with a GE Phoenix c/tome/x scanner (all scans 200 kV, 80 mA, voxel size = 0.24x0.24x0.24 mm). For the reconstruction, primarily the bones of the left side and axial skeleton (Appendix 1 for complete list) were segmented from the scans in Mimics 16.0 software (Materialise NV, Leuven, Belgium), to export .stl files representing each bone. In the case of multiple scans for individual bones (the skull and all long bones), multiple .stl files were exported, which were then merged in Meshlab 1.3.3 software (Visual Computing Lab, ISTI – CNR, Pisa, Italy) using the "Align" function. Where bones from the right side were used, these were mirrored to the left side in Meshlab to produce a complete left side of the skeleton.

The missing thoracic vertebrae T1, T5, and T7 were copied from the adjacent T2, T4, and T6 bones, respectively, as these were determined to be most similar in other felids (Randau et al., 2016). Vertebra number T10 is not present in the specimen, so this vertebra was replaced with the T10 of another specimen (LACMP 2458-19) of comparable size. The remainder of the bones from the left hand side (manus, pes, sternum, ribs, caudal vertebrae) were segmented from an Asian lion

(*Panthera leo persica*) that had been scanned at the Royal Veterinary College using a Lightspeed Pro 16 CT scanner (GE Medical Systems) to obtain helical scans for the individual limbs and vertebral column (120 kV, 100 mA; resolution of 0.96x0.96x1.25 mm), and scaled isometrically from the 133 kg Asian lion to the estimated 207 kg body mass for this specimen of *P. atrox* (average from condylobasal length of 0.326 m (Mazák et al., 2011) and femoral length of 0.404 m – from the all-carnivoran equation (Anyonge, 1993), estimates of 195 kg and 219 kg, respectively). These methods were chosen rather than using bone circumferences as it has been noted that *P. atrox* has relatively robust bones for their length (Sorkin 2008), and using the felid-specific equations from Anyonge (1993) lead to estimates of maximal *P. atrox* masses potentially exceeding 600 kg. Recent works produce much lower maximal body mass estimates for *P. atrox* (Sorkin, 2008 – 420 kg; Christiansen and Harris, 2009 – 351 kg). Whilst there are issues with averaging two bivariate regressions (for an in depth discussion Smith, 2002 and references contained therein), we do not know which of the regressions is more reliable so we used the average of the two regressions as a guide. Those regressions' estimates of 195 kg and 219 kg body mass differ by about 12%, which we viewed as plausibly close enough to warrant averaging them, given other potential sources of biological variation and methodological errors.

The finished .stl files for all of the bones were imported into Meshmixer 10.9.332 software (Autodesk, Inc.) where they were all manually aligned into a biologically plausible position based on the approximate standing posture of extant felids. The complete limbs were mirrored to create the right side and then aligned to the skeleton.

The Asian lion (National Museums of Scotland specimen NMS.Z.2015.128) was CT scanned with the muscles intact, and, despite having no contrast staining with Lugol's iodine (Kelly, 1961; Jeffery et al., 2011), we were able to segment all of the muscles from the left limbs (Figure 1). We were not able to segment the individual muscles of the vertebral column, so a gross segmentation of the cervical, thoracic, and lumbar regions of muscles was conducted. Using the scaling equations (inserting the 207 kg body mass estimate) from Cuff et al. (2016a, 2016b), the muscle belly length (i.e., length of the main striated muscle portion of the muscle-tendon unit, along its line of action) for each of the muscles was estimated for *Panthera atrox*. The expected muscle masses were also calculated from the Cuff et al. (2016a, 2016b) non-phylogenetic scaling equations (Appendices 2-13). The dataset from Cuff et al. (2016a, 2016b) has no large non-pantherine species and as such using the phylogenetic correction would likely reduce any real allometric signals; this could be particularly problematic due to *P. atrox* being a very large felid. Regardless, most muscle lengths and masses across the postcrania of felids scale (indistinguishable from) isometrically – whether or not phylogeny is accounted for – so the results are unlikely to differ greatly depending on which equation is chosen. The segmented muscles were individually scaled to match the predicted muscle length. Because the mass for each muscle and the corresponding .stl file was known from dissection of the *P. leo* specimen, and mass is proportional to volume (assuming density is the same for both muscles), after the length was scaled the two remaining dimensions were then scaled identically so the mass of each muscle matched that predicted from the scaling equations:

$$\text{Eq 1: } \text{Mass}_{\text{P. atrox}} = \text{Mass}_{\text{P. leo}} \times \text{length scale factor} \times \text{width scale factor}^2$$

This method was repeated for any tendons, where possible. However, the soft tissue contrast in the microCT scan images was often insufficient to separate tissues in the distal limbs, particularly for the long and relatively thin tendons. Thus most of the distal muscles lacked complete tendons in the resulting .stl files. For those distal muscles for which there were no easily segmented tendons, the tendons were recreated by extending a section of the muscle belly so that the length and mass of each tendon matched the mean lengths and masses expected from the scaling equations of Cuff et al. (2016a, 2016b). All of the scaled muscles and tendons were then placed on the left side of the *P. atrox* reconstructed skeleton in the appropriate positions using any evident muscle scarring patterns on the bones and the origins and insertions observed during dissections of extant species, before mirroring to the right side (as with the bones) in Meshlab.

We attempted to compare the body and segment mass estimates from convex hull models based on the reconstructions using just the skeleton and using the fully-fleshed model. This was done by using the "convex hull" filter within Meshlab for the skeletal elements from each of the body segments (e.g., Basu et al., 2016). Body mass estimates were calculated from the sum of all masses from the complete set of convex hulls using a

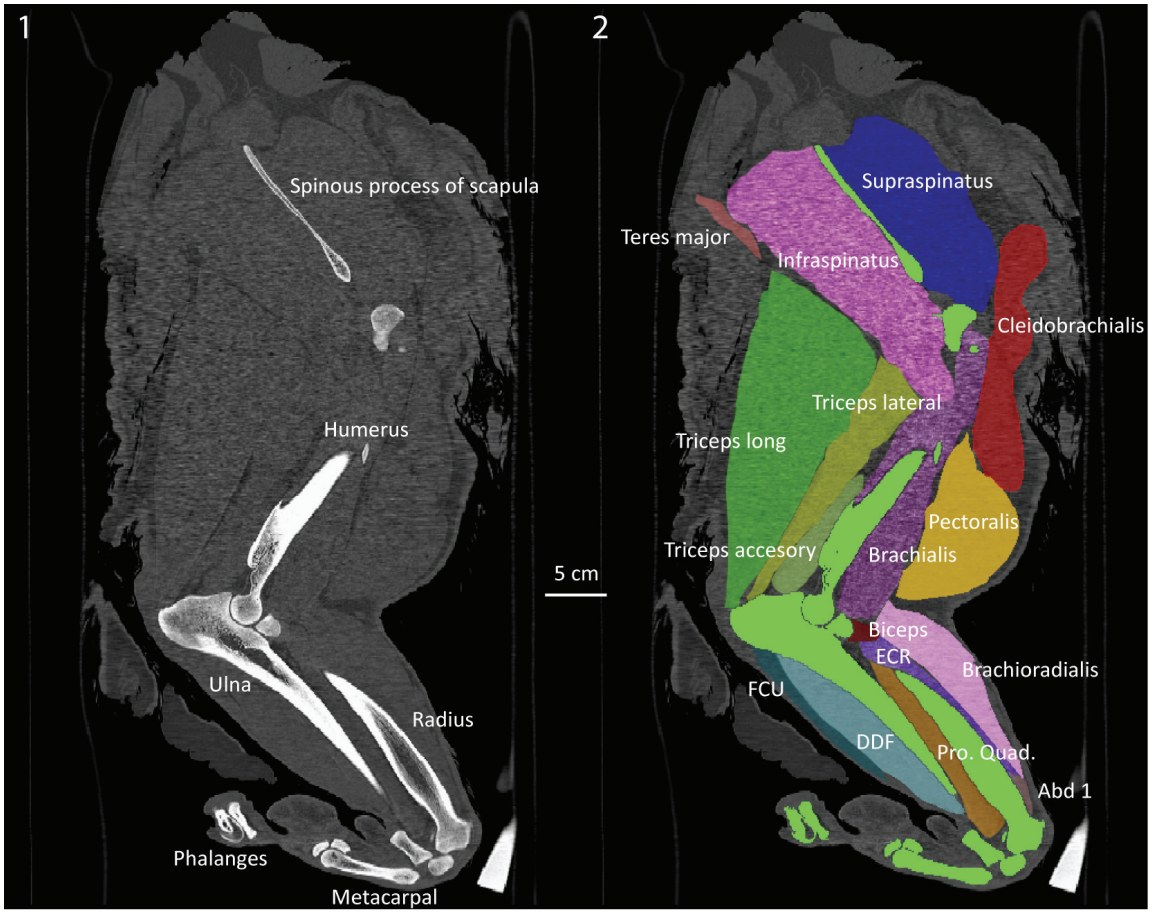

FIGURE 1. CT scan slice showing an approximately mediolateral view (i.e., longitudinal section) of an Asian lion's forelimb. **1,** Dark grey is adipose and connective tissues, lighter grey is muscles, white is bone. Bottom right corner white is a density calibration phantom (1.69 g cm^{-3}; "cortical bone"). **2,** Segmentation of the lion forelimb with select muscles highlighted. Abbreviations: FCU – flexor carpi ulnaris; DDF – deep digital flexors; ECR – m. extensor carpi radialis; Pro Quad – m. pronator quadratus; Abd1 – m. abductor digiti I.

range of densities from 893.36 kg m^{-3} multiplied by 1.091 to 1.322 (i.e., 974.7 kg m^{-3} to 1181 kg m^{-3} – a correction factor due to the underestimation of limb masses) (Sellers et al., 2012). In addition to total body mass estimations, convex hull estimates were made of the individual limb segments and compared to the values from the reconstructions. Finally estimations of segment masses were carried out using the same convex hull methods, but applied to the fully fleshed model for the limb segments rather than to the isolated bones. These data were validated by repeating the methods for a modern lion's left limbs, with the total volumes for each limb segment being isolated from CT scan data, and multiplied by a density of 1060kg m^{-3}.

RESULTS AND DISCUSSION

Although the resulting skeletal reconstruction was, necessarily, a composite using some elements from either another *Panthera atrox* individuals or the cadaver of *P. leo*, it is the most complete scientific reconstruction of a single *P. atrox* specimen to date (Figure 2). Combined with the skeletal reconstruction, dissections of related species, and recent analyses of felid muscle scaling, the muscles could be reconstructed (Tables 1-3) and placed onto the skeleton (Figure 3). As somewhat of a "best case" scenario for reconstructing an extinct animal's morphology, we used the musculature of a modern lion (phylogenetically the closest relative of *P. atrox* among extant felids, with less than 1.89 Ma separating them) and scaled the muscles to the predicted size using the scaling

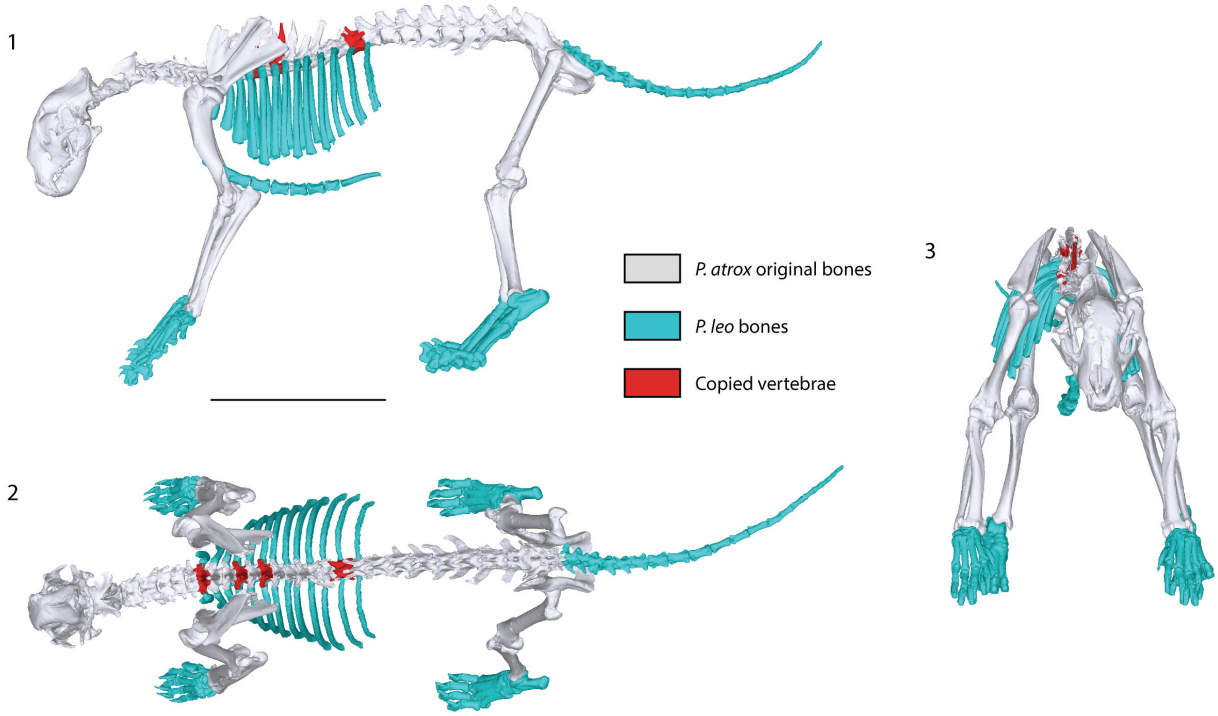

FIGURE 2. Skeletal reconstruction showing the original bones from *Panthera atrox* and those which have been copied from other vertebrae (red), or from *P. leo persica* (blue). **1,** lateral; **2,** dorsal; **3,** anterior views. Scale bar is 50 cm.

equations. These muscles, when scaled, generally matched the osteology very well (e.g., the scapular muscles of the m. infraspinatus and m. supraspinatus tightly bound by spinous process of the scapula, or the limb muscles closely wrapping the bones without intersecting each other or the bones). This good fit of the muscles to the skeleton might not be the case if the reconstructions were carried out on more distantly related taxa such as *Smilodon*, which is separated from all extant felids by >20 Ma. Nonetheless, this whole-body reconstruction allowed presumably improved estimates of body segment dimensions (e.g., masses, centres of mass, moments of inertia) for this individual, and could also be applied to related species in the future.

The muscle reconstructions were derived in part from body mass, so they will be sensitive to which method is used to estimate body mass. The 207 kg body mass used here was derived from equations that give mass estimates from 195-219 kg – a range of 24 kg (around 12% of body mass). Using the two estimates for body mass, the calculated estimates for muscle and tendon length differed by around 4%, and the muscle and tendon masses varied by around 12%. However, the source of greater uncertainty in the muscle and tendon estimates was the scaling equations, which for some metrics had particularly large error margins (linked to the small number of individuals sampled by Cuff et al., 2016a, 2016b). For those muscles, unrealistic predictions may occur (Appendices 2-13 for 95% confidence intervals for all muscles and tendons). *Post hoc* adjustments were made for those muscles by using the origin and insertion points to obtain lengths that matched the skeleton best. In particular, the m. brachioradialis muscle's belly length was predicted to be 2.41 m long (Table 1), but from insertion and origination points was actually reconstructed at 0.275 m long, and the m. rectus femoris tendon length was predicted to be 0.65 m long, but was reconstructed as 0.060 m. This is also the case with some of the vertebral muscles (e.g., the estimated length of m. semispinalis capitis biventer was almost double the length of the entire *Panthera atrox* skeletal reconstruction), but the individual vertebral muscles could not be individually segmented from the CT scans.

Our method developed here for whole-body reconstruction of *Panthera atrox* is based on the usage of scaling equations that relate bone dimensions and body mass, permitting estimation of the latter. These equations have been shown to be

TABLE 1. Forelimb muscle belly and tendon lengths and masses as predicted from Cuff et al. (2016a). Serrat. vent. cerv. = m. serratus ventralis cervicus, Serrat. vent. thor. = m. serratus ventralis thoracis, Abd. dig. 1 = m. abductor digiti 1. Ext. = extensor, Flex. = flexor.

Muscle	Belly length (m)	Tendon length (m)	Belly mass (kg)	Tendon mass (kg)
Latissimus dorsi	0.646		1.776	
Trapezius cervicis	0.379		0.229	
Trapezius thoracis	0.275		0.242	
Rhomboideus capitis	0.428		0.232	
Rhomboideus cervicis	0.230		0.444	
Rhomboideus thoracis	0.204		0.156	
Omotransversarius	0.350		0.169	
Cleidocephalicus	0.405		0.484	
Cleidobrachialis	0.336	0.140	0.509	
Serrat. vent. cerv.	0.244		0.523	
Serrat. vent. thor.	0.240		0.552	
Pectoralis superficialis	0.372		0.567	
Pectoralis profundus	0.642		1.923	
Supraspinatus	0.344	0.045	1.001	0.001
Infraspinatus	0.261	0.203	0.699	0.038
Deltoideus acromion	0.184		0.162	
Deltoideus spinous	0.195	0.113	0.190	0.000
Teres major	0.286	0.002	0.554	0.001
Subscapularis	0.254	0.022	0.670	1.000
Teres minor	0.091		0.035	
Coracobrachialis	0.644		0.133	
Triceps longus	0.348	0.130	1.562	0.006
Triceps lateralis	0.277	0.101	0.582	0.005
Triceps medius	0.253	0.136	0.197	0.010
Triceps accessory	0.281		0.123	
Biceps brachi	0.257	0.102	0.531	0.012
Brachialis	0.297	0.059	0.138	0.003
Anconeus	0.165		0.072	
Ext. carpi radialis	0.310	0.163	0.201	0.008
Ext. digitorum communis	0.236	0.014	0.186	0.074
Ext. digitorum lateralis	0.415	0.169	0.054	0.008
Ext. carpi ulnaris	0.264	0.163	0.077	0.005
Flex. carpi ulnaris ulnar	0.262	0.021	0.139	0.003
Flex. carpi ulnaris humeral	0.295	0.108	0.162	0.002
Brachioradialis	2.410		0.218	
Supinator	0.147	0.002	0.039	0.004
Pronator teres	0.216		0.128	
Pronator quadratus	0.254	0.073	0.071	0.004
Flex. carpi radialis	0.259	0.081	0.058	0.002
Flex. digitorum complex	0.284	0.177	0.499	0.087
Abd. dig. 1	0.418	0.223	0.039	0.003

TABLE 2. Hindlimb muscle belly and tendon lengths and masses as predicted from Cuff et al. (2016b). Gastroc. = gastrocnemius, Dig. = digitorum, Supefic. = superficialis.

Muscle	Belly length (m)	Tendon length (m)	Belly mass (kg)	Tendon mass (kg)
Biceps femoris	0.420		1.537	
Caudofemoralis	0.373	0.345	0.515	0.019
Sartorius	0.654		0.775	
Tensor fascia latae	0.190	0.293	0.542	0.043
Vastus lateralis	0.389		0.962	
Rectus femoris	0.419	0.650	0.693	0.079
Vastus medius	0.350	0.029	0.487	0.004
Vastus intermedius	0.486	0.002	0.168	0.000
Semitendinosus	0.464	0.134	0.684	0.005
Semimembranosus	0.718	0.043	1.369	0.003
Gracilis	0.257	0.088	0.534	0.016
Gluteus superficialis	0.184		0.153	
Gluteus medius	0.249		1.063	
Gluteus profundus	0.231	0.005	0.090	0.001
Piriformis	0.090	0.023	0.093	0.002
Gemelli	0.154		0.146	
Quadratus femoris	0.125		0.046	
Obturator externus	0.124		0.168	
Obturator internus	0.118	0.078	0.178	0.008
Pectineus	0.268		0.093	
Adductor magnus	0.392		1.181	
Adductor brevis	0.214		0.211	
Iliacus	0.564		0.538	
Psoas major	0.558	0.058	0.785	0.074
Psoas minor	0.373	0.072	0.242	0.002
Gastroc. lateralis	0.334	0.072	0.377	0.021
Gastroc. medius	0.291	0.137	0.302	0.021
Superfic. dig. flexor	0.293	0.373	0.119	0.311
Soleus	0.268	0.024	0.123	0.002
Dig. extensor longus	0.291	0.269	0.084	0.105
Tibialis cranialis	0.284	0.111	0.213	0.004
Popliteus	0.189	0.095	0.054	0.003
Dig. extensor lateralis	0.215	0.320	0.026	0.003
Peroneus longus	0.222	0.166	0.185	0.062
Peroneus brevis	0.200	0.242	0.041	0.004
Deep digital flexor medial	0.298	0.299	0.165	0.062
Deep digital flexor lateral	0.324	0.465	0.137	0.040
Tibialis caudalis	0.272	0.180	0.117	0.011

TABLE 3. Vertebral muscle belly and tendon lengths and masses as predicted from Cuff et al. (2016a, b). Longis. = longissimus, Iliocost. = iliocostalis, Multifid. = multifidus.

Muscle	Belly length (m)	Tendon length (m)	Belly mass (kg)	Tendon mass (kg)
Rectus capitis	0.112		0.098	
Splenius cervicis	0.395		0.366	
Serratus dorsalis cranialis	0.127	0.228	0.124	0.033
Serratus dorsalis caudalis	0.085	0.001	0.080	0.020
Semispinalis capitis biventer	4.009		0.325	
Semispinalis capitis complexus	0.470		0.325	
Spinalis cervicis	0.314		0.336	
Spinalis thoracis	0.641		0.877	
Longissimus capitis	0.323		0.064	
Longissimus cervicis	0.405		0.143	
Longissimus thoracis	0.827		0.916	
Iliocostalis thoracis	0.640		0.195	
Multifidis throacis	0.713		0.355	
Longis. lumborum	2.342		0.987	
Iliocost. lumborum	1.494		0.630	
Multifid. lumborum	0.381		0.661	

very good ($r^2 > 0.95$) at estimating body masses for extant *Panthera* species (Anyonge, 1993; Mazák et al., 2011) and by using them we also produced a reasonable estimation for body composition (Table 4) compared to modern *P. leo*. The musculature of extant lions accounts for (on average) 57.1% of total body mass, then the remainder of body mass is 11.5% skin, 12.4% skeleton, 11.8% organs, about 4.6% blood and waste, and 2.7% fat (Davis, 1962). For *P. atrox*, the muscles and their respective tendons reconstructed from the scaling equations of Cuff et al. (2016a, 2016b) correspond to 84.4 kg in mass (40.8% of total body mass calculated from the bone regression). Of course, other muscles (e.g., abdominal, intercostal, hyomandibular, and various intrinsic muscles of the manus, pes, and skull) would add to the muscle mass further. However, it would be surprising if there was another 16.3% of body mass in this remaining musculature as this musculature only corresponds to approximately 2-3% of total mass in domestic cats (Grand, 1977). This discrepancy may be due to the different methods of preparation between Cuff et al. (2016a, 2016b), where individual muscles were dissected, and Davis (1962), which does not appear to have removed extraneous connective tissues and intermuscular adipose tissues. This suggestion is somewhat supported by the relatively low body fat content of lions (2.7%) estimated by Davis (1962), relative to those reported for other felid species for which data are available (domestic cat: 20.9% (Lauten et al., 2000) – 24.4% (Munday et al., 1994); *Lynx* spp. 15 – 16% (Pitts and Bullard, 1968)).

Convex hull models have been used recently to reconstruct body segmental shapes and estimate body masses for skeletons with no preserved soft tissues (e.g., Sellers et al., 2012; Basu et al., 2016; Bates et al., 2016; Brassey et al., 2016). The convex hull model for the entire skeleton of *P. atrox* produced a volume of 0.185 m^3 (Figure 4). Using the range of potential densities (Sellers et al., 2012), the body mass estimates varied from 180 kg to 219 kg. The mid-point of these two extreme ranges is 200 kg, only a few kilograms away from the ~207 kg estimate obtained from the bones, which is unsurprising as the composite bones were scaled to the 207 kg estimate. However, as convex hulls tend to underestimate total volumes, methods for estimating masses from them are heavily reliant on the density values used (e.g., a density of 1359 kg m^{-3} from Brassey and Sellers (2014), which they calculated to be the apparent density for convex hull models for non-primate mammals, would produce a very different estimate of 251 kg for the uncorrected convex hull of this *Panthera atrox* specimen). Whilst convex hull models can produce realistic estimates for total mass, they will produce

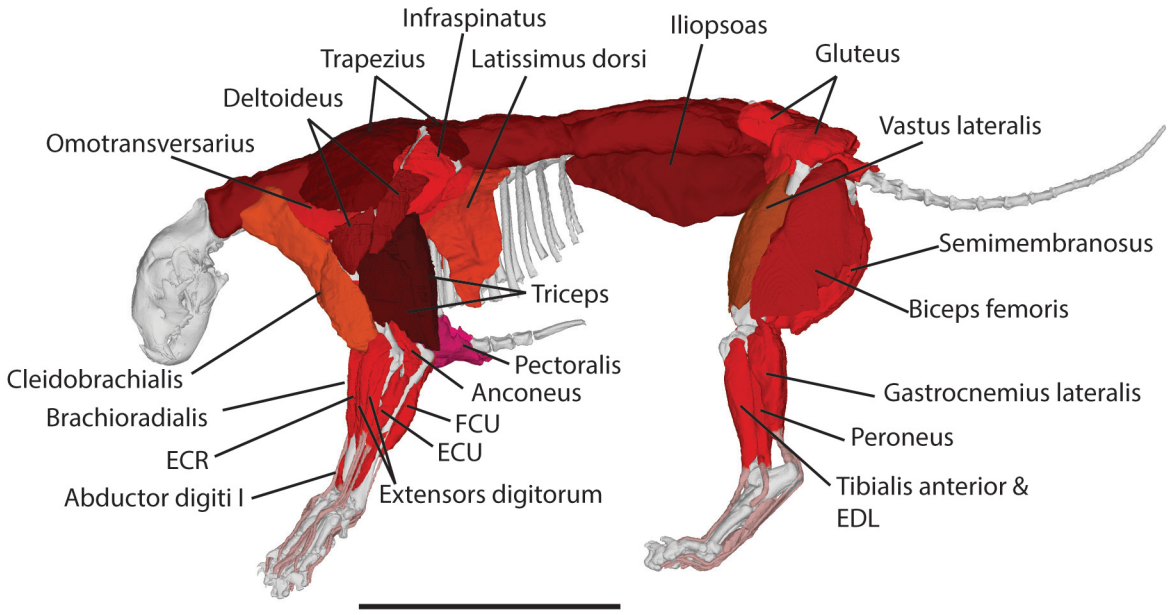

FIGURE 3. Muscled reconstruction of *Panthera atrox* showing the major muscle groups in lateral view. Abbreviations: FCU – m. flexor carpi ulnaris; ECU – m. extensor carpi ulnaris; ECR – m. extensor carpi radialis; EDL – m. extensor digitorum longus. Scale bar is 50 cm.

regional variability, with the limb masses generally underestimated, and the core body overestimated (Sellers et al., 2012; Brassey and Sellers, 2014). The muscled reconstruction of *P. atrox* showed how much variability was obtained for the limb morphology (Figure 5).

On the modern lion, convex hull-based models of the bones produced segmental estimates that were up to 3.7 times and 5.23 times smaller than the masses of the muscles and bones in the proximal sections of the fore- and hindlimbs, respectively (Table 5). However, using reconstructed muscles and bones together still underestimated total limb mass by a factor of 1.3-1.8 (Table 5) due to the lack of connective tissues, blood vessels, nerves, adipose tissue, and skin. This discrepancy could be compensated for by producing a convex hull model of the limb over the muscled reconstructions, which produced mass estimates that were within 8% of the actual fleshed limb segments (Table 5), rather than producing the original ~30-80% underestimates.

For any biomechanical model of a species it is important to understand more than just the masses of the segments, but also the segmental centres of mass and moments of inertia, all of which determine how the segments might have moved (Allen et al., 2009, 2013). The convex hull models of the muscled limb segments for *Panthera leo* produced centre of mass (COM) estimates that were very close to those from CT scan segmentation in terms of absolute distances, and percentages of segment length (Table 6), suggesting this method of recon-

TABLE 4. Body composition of *Panthera atrox* from reconstructed muscles and dissections of extant *P. leo* specimens (Davis, 1962). "Muscle recon" is the sum of the reconstructed forelimb, hindlimb, and vertebral muscles. Additional muscle is the remaining expected muscle using the body compositions for modern lions (Davis, 1962) i.e., 57.1% - "Muscle recon".

	Body	Forelimb muscles	Hindlimb muscles	Vertebral muscle	Muscle recon	Additional muscle	Bone	Adipose	Organs	Skin and fur	Blood and waste
Mass (kg)	207	35.2	32.2	16.9	84.4	33.7	25.7	5.5	24.4	23.8	9.56
Percentage (%)	100	17.0	15.6	8.18	40.8	16.3	12.4	2.67	11.8	11.5	4.62

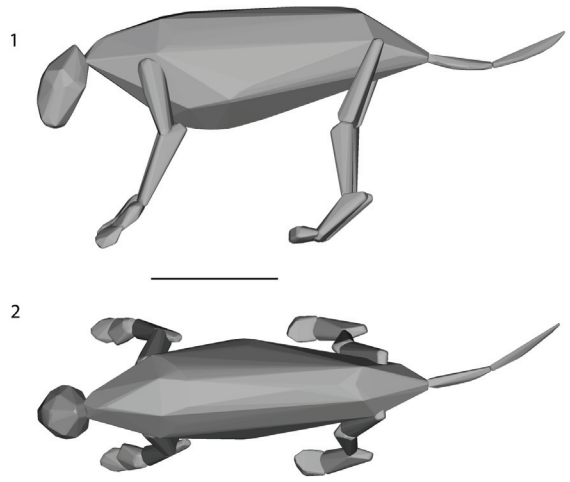

FIGURE 4. Convex hull model from the reconstructed *Panthera atrox* skeleton shown in Figure 2. **1,** left lateral view; **2,** dorsal view. Scale bar is 50 cm.

structing limb segments is comparable to the original fleshed limb.

From our reconstructions of the limb segments for *Panthera atrox*, the mass estimates from the convex hulls over the bones relative to the muscle and bone masses are comparable to those of *P. leo* (Tables 5 and 7). This result supports the conclusion that the convex hulls over the reconstructed muscles will also be similarly accurate for *P. atrox* as they were for *P. leo*. For the hindlimbs, the percentage of the total mass for each segment was very similar to those of domestic cats, but the forelimb segments in *P. atrox* were almost double the typical mass measured in domestic cats (Grand, 1977). As the muscle masses appear to scale isometrically in the forelimbs of felids (Cuff et al., 2016a) and there is only a few percentage points difference (in terms of total body mass) between the forelimb muscles of *P. atrox* and domestic cats, this increase in mass is probably

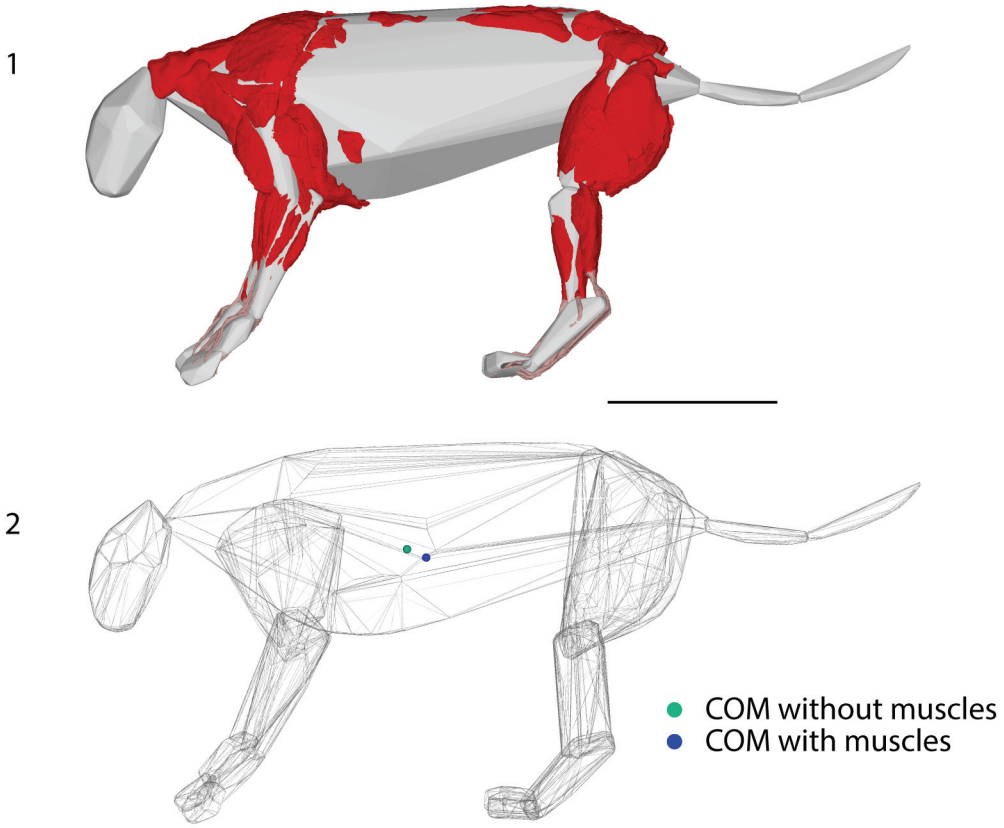

FIGURE 5. *Panthera atrox* reconstruction showing differences between simple convex hulls and more complex reconstructions. **1,** Reconstructed muscles overlaid on the convex hull of just the bones. Any muscles that are visible extend beyond the range of the convex hull, thereby demonstrating the underestimation of size by convex hulls based solely on bones. **2,** Reconstructions showing the posteroventral movement of the centre of mass (COM) between the bone convex hull and the muscled convex hull models of *Panthera atrox*. Scale bar is 50 cm.

TABLE 5. *Panthera leo* limb segment masses from the different mass estimate methods. "Flesh" is the weight calculated for the segment volumes (multiplied by 1060 kg m^{-3}) from CT segmentation. "Reconstruction" was based on the muscle and bone reconstruction, although muscle masses for the manus and pes were calculated as total tendon mass for distal muscles. Convex hull bones ("CHB") is the convex hull range of masses and the convex hull muscles ("CHM") is the convex hull range of masses from the muscled reconstructions. The masses for both convex hull methods were calculated from the volumes using only the mean density [893.36 kg m^{-3} multiplied by 1.206 (Sellers et al., 2012)]. Ratios of each of these estimates are shown in the final four columns on the right side of the table. Dig_Man = digits of the manus, Dig_Pes = digits of the pes.

		Reconstruction			CHB	CHM	Flesh/	Recon/	CHM/	Flesh/
	Flesh	Bone mass	Muscle mass	Total	Mean	Mean	Recon	CHB	Recon	CHM
Humerus	7.47	0.44	3.94	4.38	1.19	7.29	1.71	3.69	1.67	1.02
Ulna/Radius	2.39	0.16	1.40	1.56	0.86	2.25	1.53	1.81	1.44	1.07
Manus	0.55	0.18	0.29	0.47	0.42		1.18	1.12		
Dig_Man	0.44	0.07		0.07	0.29		6.16	0.24		
Femur	10.9	0.62	7.23	7.85	1.50	10.6	1.39	5.23	1.35	1.03
Tibia	2.35	0.53	1.13	1.66	1.28	2.54	1.41	1.30	1.53	0.92
Pes	0.75	0.41	0.27	0.68	0.73		1.10	0.93		
Dig_Pes	0.30	0.13		0.13	0.29		2.31	0.45		

TABLE 6. Centre of mass (COM) validation test for extant lion limb segments. "Original COM" was derived from CT scan data for each segment, "CHM COM" from the convex hull models fitted to the muscled limbs, and "Difference" is the "Original COM" minus "CHM COM". Italicised numbers are long axis lengths from which the percentage (%) of segment lengths were calculated. Positive x, y, and z are anterior, dorsal, and medial, respectively, relative to the origin at the proximal end of the segment. Centre of mass (COM) was expressed as % of length (from the proximal end) relative to the total proximodistal length of the segment.

	Original COM			CHM COM			Difference			Original % of length	CHM % of length
	x	y	z	X	y	z	x	y	z		
Humerus	0.0003	-0.1120	0.005226	-0.0067	-0.1223	0.011691	0.0070	0.0103	-0.0065	45.6	49.8
Ulna/Radius	-0.0023	-0.1093	0.001969	0.0016	-0.0935	0.002054	-0.0038	-0.0158	-0.0001	42.7	36.6
Femur	-0.0201	-0.0943	-0.0177	-0.0164	-0.1098	-0.0216	-0.0037	0.0154	0.0039	32.1	37.4
Tibia	-0.0219	-0.1497	-0.0004	-0.0230	-0.1607	-0.0009	0.0011	0.0111	0.0005	50.3	54.0

linked to an increase in robustness of the bones (Sorkin, 2008; Doube et al., 2009) and may be correlated with the importance of the forelimbs to tackle prey in larger felids (Meachen-Samuels and Van Valkenburgh, 2009). Considering the close concordance of centres of mass between the segmental convex hull reconstructions of *P. leo* and its CT scan segmentation (Table 6), we can confidently reconstruct the limb segment COMs of *P. atrox* (Table 8), as well as the moments of inertia (Table 9). Additionally, we seemed to be able to more accurately estimate whole body COM, which is more posteroventrally located (5.2 cm posteriorly, 3.1 cm ventrally) in the muscled convex hull models than in models using just the skeleton (Figure 5). By using empirical data from extant lions and other felids to reconstruct the muscles (and thus body segments) quantitatively, we were better able to reconstruct this fossil taxon in detail that was previously unobtainable.

CONCLUSIONS

Our microCT scan data from one very complete skeletal specimen enabled a new reconstruction of *Panthera atrox* in more complete detail than before, although where there were incomplete data we had to use portions of closely related taxa, and thus our reconstruction is still a composite. Using data derived from dissections of extant felids spanning a range of body masses, it was possible to use regressions to estimate the size of the locomotor musculature of this specimen of *P. atrox*. These reconstructions allowed for more accurate esti-

TABLE 7. Reconstructed and convex hull masses for various segments of the body of Panthera atrox. Bone mass was calculated from estimated bone density (1150 kg m^{-3}) based on relative bone mass (25.7 kg - Table 4) divided by total bone volume (0.0223 m^3). Muscle mass was calculated from the muscle and tendon that forms the majority of the segment (e.g., M. biceps brachii has tendons that extend to the scapula and the ulna, but these are all counted to the mass of the humeral segment as that is the majority of the muscle and tendon) (Tables 1-3), with tendons for the distal muscles being placed in the manus and pes segments. Convex hull bones' (CHB) and convex hull muscles' (CHB) masses were calculated from the volumes multiplied by relative density (893.36 kg m^{-3} multiplied by 1.091, 1.206, and 1.322 (Sellers et al., 2012) respectively). Dig_Man and Dig_Pes are the digits for the manus and pes, respectively. The Recon/CHB is the ratio of reconstructed mass to CHB mass, and CHM/Recon is the ratio of the CHM mass to the reconstructed mass. Rad = radius, Dig_Man = digits of the manus, Fib = fibula, Dig_Pes = digits of the pes.

	Reconstruction			Convex Hull Bones			Convex Hull Muscles				
	Bone Mass	Muscle Mass	Total	Mean	Lower	Upper	Mean	Lower	Upper	Recon/CHB	CHM/Recon
Humerus	1.03	7.65	8.88	2.88	2.60	3.15	10.16	9.19	11.14	3.02	1.17
Ulna/Rad	0.73	1.94	2.67	2.03	1.83	2.22	4.44	4.02	4.87	1.32	1.66
Manus	0.34	0.20	0.54	0.92	0.84	1.01	1.28	1.16	1.40	0.59	2.35
Dig_Man	0.17		0.17	0.60	0.55	0.66	0.70	0.63	0.76	0.28	4.12
Femur	1.12	13.5	14.63	2.90	2.62	3.18	17.60	15.92	19.29	5.05	1.20
Tibia/Fib	0.87	1.99	2.86	1.89	1.71	2.07	4.33	3.92	4.75	1.51	1.52
Pes	0.90	0.61	1.50	1.60	1.45	1.76	2.16	1.96	2.37	0.94	1.44
Dig_Pes	0.28		0.28	0.68	0.62	0.75	0.92	0.83	1.01	0.41	3.27

TABLE 8. Centre of mass for *Panthera atrox* limb segments. Positive x, y, and z are anterior, dorsal, and medial, respectively, relative to the origin at the proximal end of the segment. Centre of mass (COM) was expressed as % of length (from the proximal end) relative to the total proximodistal length of the segment.

Segment	x	y	z	COM % of length
Humerus	0.002	-0.119	0.009	0.372
Ulna	-0.002	-0.117	0.001	0.360
Manus	-0.010	-0.118	-0.001	0.622
Digits	-0.015	-0.045	-0.009	0.414
Femur	-0.012	-0.144	-0.018	0.380
Tibia	-0.017	-0.200	-0.014	0.537
Pes	-0.020	-0.114	-0.010	0.464
Digits	0.001	-0.045	-0.017	0.370

TABLE 9. Moments of inertia (relative to the centre of mass; Table 8) for the limb segments of *Panthera atrox*. Units are kg m^2.

Humerus			Ulna			Manus			Digits		
x	y	z	x	Y	z	x	y	z	x	y	z
0.1068	0.0616	0.1476	0.0551	0.0081	0.0576	0.0040	0.0015	0.0034	0.0012	0.0007	0.0010

Femur			Tibia			Pes			Digits		
x	y	z	x	Y	z	x	y	z	x	y	z
0.3373	0.1221	0.4066	0.0460	0.0085	0.0482	0.0151	0.0025	0.0150	0.0020	0.0011	0.0015

mates of limb masses (and the centre of masses of individual segments) from convex hull modelling than previous methods using just the bones. We supported this presumption by conducting validation tests on a modern lion's body segments, using multiple methods. By doing the reconstructions of the skeleton, segmental inertial properties, and in combination with the musculature data, it was possible to create a full musculoskeletal reconstruction. In addition, our reconstructions of the musculature allow for body composition estimates for *P. atrox* for the first time. Whilst the reconstruction here was carried out mainly in freely available software (e.g., Meshlab) with licensed software used only for the CT scan segmentation, it is entirely possible to carry out future reconstructions only in open source software (e.g., SPIERS; Sutton et al., 2012), expanding the accessibility of this methodology to researchers worldwide.

ACKNOWLEDGEMENTS

This work was funded by Leverhulme Trust grant RPG 2013-124 to A. Goswami (UCL) and J.R. Hutchinson (RVC). We thank M. Randau (UCL) for preliminary assessment of the specimen, A. Farrell from The George C. Page Museum, and G. Takeuchi and L. Chiappe from the NHMLA for allowing access to this specimen and facilitating its loan for scanning, and N. Ives and G. Stupian from The Aerospace Corporation for scanning this specimen. We finally thank two anonymous reviewers for their comments that improved this paper.

REFERENCES

Allen, V., Bates, K.T., Li, Z., and Hutchinson, J.R. 2013. Linking the evolution of body shape and locomotor biomechanics in bird-line archosaurs. *Nature*, 497:104-107. doi:10.1038/nature12059

Allen, V., Paxton, H., and Hutchinson, J.R. 2009. Variation in center of mass estimates for extant sauropsids and its importance for reconstructing inertial properties of extinct archosaurs. *The Anatomical Record,* 292:1442-1461. doi:10.1002/ar.20973

Anyonge, W. 1993. Body mass in large extant and extinct carnivores. *Journal of Zoology*, 231:339-350. doi:10.1111/j.1469-7998.1993.tb01922.x

Barnett,R., Mendoza, M.L.Z., Soares, A.E.R., Ho, S.Y.W., Zazula, G., Yamaguchi, N., Shapiro, B., Kirillova, I.V., Larson, G., and Gilbert, M.T.P. 2016. Mitogenomics of the extinct cave lion, *Panthera spelaea* (Goldfuss, 1810), resolve its position within the *Panthera* cats. *Open Quaternary*, 2. doi:10.5334/oq.24

Barnett, R., Shapiro, B., Barnes, I., Ho, S.Y., Burger, J., Yamaguchi, N., Higham, T.F., Wheeler, H.T., Rosendahl, W., Sher, A.V., Sotnikova, M., Kuznetsova, T., Baryshnikov, G.F., Martin, L.D., Harington, C.R., Burns, J.A., and Cooper, A. 2009. Phylogeography of lions (*Panthera leo ssp.*) reveals three distinct taxa and a late Pleistocene reduction in genetic diversity. *Molecular Ecology*, 18:1668-1677. doi:10.1111/j.1365-294X.2009.04134.x

Basu, C., Falkingham, P.L., and Hutchinson, J.R. 2016. The extinct, giant giraffid *Sivatherium giganteum*: skeletal reconstruction and body mass estimation. *Biology Letters*, 12. doi:10.1098/rsbl.2015.0940

Bates, K.T., Mannion, P.D., Falkingham, P.L., Brusatte, S.L., Hutchinson, J.R., Otero, A., Sellers, W.I., Sullivan, C., Stevens, K.A., and Allen, V. 2016. Temporal and phylogenetic evolution of the sauropod dinosaur body plan. *Royal Society Open Science*, 3:150636.

Bates, K.T., Manning, P.L., Hodgetts, D., and Sellers, W.I. 2009. Estimating mass properties of dinosaurs using laser imaging and 3D computer modelling. *PLoS ONE*, 4:e4532. doi:10.1371/journal.pone.0004532

Brassey, C.A. and Sellers, W.I. 2014. Scaling of convex hull volume to body mass in modern primates, non-primate mammals and birds. *PLoS ONE*, 9:e91691. doi:10.1371/journal.pone.0091691

Brassey, C.A., O'Mahoney, T.G., Kitchener, A.C., Manning, P.L., and Sellers, W.I. 2016. Convex-hull mass estimates of the dodo (*Raphus cucullatus*): application of a CT-based mass estimation technique. *PeerJ,* 4:e1432.

Bryant, H.N. and Seymour, K.L. 1990. Observations and comments on the reliability of muscle reconstruction in fossil vertebrates. *Journal of Morphology*, 206:109-117. doi:10.1002/jmor.1052060111

Christiansen, P. and Harris, J. 2009. Craniomandibular morphology and phylogenetic affinities of *Panthera atrox*: implications for the evolution and paleobiology of the lion lineage. *Journal of Vertebrate Paleontology*, 29:934-945.

Cuff, A.R. and Rayfield, E.J. 2015. Retrodeformation and muscular reconstruction of ornithomimosaurian dinosaur crania. *PeerJ*, 3:e1093. doi:10.7717/peerj.1093

Cuff, A.R., Sparkes, E.L., Randau, M., Pierce, S.E., Kitchener, A.C., Goswami, A., and Hutchinson, J.R. 2016a. The scaling of postcranial muscles in cats (Felidae) I: forelimb, cervical, and thoracic muscles. *Journal of Anatomy*. doi:10.1111/joa.12477

Cuff, A.R., Sparkes, E.L., Randau, M., Pierce, S.E., Kitchener, A.C., Goswami, A., and Hutchinson, J.R. 2016b. The scaling of postcranial muscles in cats (Felidae) II: hindlimb and lumbosacral muscles. *Journal of Anatomy*. doi:10.1111/joa.12474

Davis, D.D. 1962. Allometric relationships in lions vs. domestic cats. *Evolution*, 16:505-514.

Doube, M., Wiktorowicz Conroy, A., Christiansen, P., Hutchinson, J.R., and Shefelbine, S. 2009. Three-dimensional geometric analysis of felid limb bone allometry. *PLoS One*, 4(3):e1742.

Fuller, B.T., Fahrni, S.M., Harris, J.M., Farrell, A.B., Coltrain, J.B., Gerhart, L.M., Ward, J.K., Taylor, R.E., and Southon, J.R. 2014. Ultrafiltration for asphalt removal from bone collagen for radiocarbon dating and isotopic analysis of Pleistocene fauna at the tar pits of Rancho La Brea, Los Angeles, California. *Quaternary Geochronology*, 22:85-98. doi:10.1016/j.quageo.2014.03.002

Grand, T.I. 1977. Body weight: its relation to tissue composition, segment distribution, and motor function. I. Interspecific comparisons. *American Journal of Physical Anthropology*, 47:211-240. doi:10.1002/ajpa.1330470204

Hutchinson, J.R., Bates, K.T., Molnar, J., Allen, V., and Makovicky, P.J. 2011. A computational analysis of limb and body dimensions in *Tyrannosaurus rex* with implications for locomotion, ontogeny, and growth. *PLoS ONE*, 6:e26037. doi:10.1371/journal.pone.0026037

Jeffery, N.S., Stephenson, R.S., Gallagher, J.A., Jarvis, J.C., and Cox, P.G. 2011. Micro-computed tomography with iodine staining resolves the arrangement of muscle fibres. *Journal of Biomechanics*, 44:189-192. doi:10.1016/j.jbiomech.2010.08.027

Kelly, F.C. 1961. Iodine in medicine and pharmacy since its discovery-1811-1961. *Proceedings of the Royal Society: Medicine*, 54:831-836.

Lauten, S.D., Cox, N.R., Baker, G.H., Painter, D.J., Morrison, N.E., and Baker, H.J. 2000. Body composition of growing and adult cats as measured by use of dual energy X-ray absorptiometry. *Comparative Medicine*, 50:175-183.

Lautenschlager, S. 2013. Cranial myology and bite force performance of *Erlikosaurus andrewsi*: a novel approach for digital muscle reconstructions. *Journal of Anatomy*, 222:260-272. doi:10.1111/joa.12000

Leidy, J. 1853. Description of an extinct species of American lion: *Felis atrox*. *Transactions of the American Philosophical Society*, 10:319-321.

Mazák, J.H., Christiansen, P., and Kitchener, A.C. 2011. Oldest known pantherine skull and evolution of the tiger. *PLoS ONE*, 6:e25483. doi:10.1371/journal.pone.0025483

Meachen-Samuels, J. and Van Valkenburgh, B. 2009. Forelimb indicators of prey-size preference in the Felidae. *Journal of Morphology*, 270:729-744. doi:10.1002/jmor.10712

Munday, H.S., Earle, K.E., and Anderson, P. 1994. Changes in the body composition of the domestic shorthaired cat during growth and development. *Journal of Nutrition*, 124:2622S-2623S.

Persons IV, W.S., Currie, P.J., and Norell, M.A. 2013. Oviraptorosaur tail forms and functions. *Acta Palaeontologica Polonica*, 59. doi:10.4202/app.2012.0093.

Pitts, G.C. and Bullard, T.R. 1968. Some interspecific aspects of body composition in mammals, p. 45-70. *Body Composition in Animals and Man*. National Academy of Science, Washington, D.C.

Randau, M., Goswami, A., Hutchinson, J.R., Cuff, A.R., and Pierce, S.E. 2016. Cryptic complexity in felid vertebral evolution: shape differentiation and allometry of the axial skeleton. *Zoological Journal of the Linnean Society*, 178:183-202. doi:10.1111/zoj.12403

Sellers, W.I., Hepworth-Bell, J., Falkingham, P.L., Bates, K.T., Brassey, C.A., Egerton, V.M., and Manning, P.L. 2012. Minimum convex hull mass estimations of complete mounted skeletons. *Biology Letters*, 8:842-845. doi:10.1098/rsbl.2012.0263

Smith, R.J. 2002. Estimation of body mass in palaeontology. *Journal of Human Evolution*, 43:271-287. doi:10.1006/jhev.2002.0573

Sorkin, B. 2008. A biomechanical constraint on body mass in terrestrial mammalian predators. *Lethaia*, 41:333-347. doi:10.1111/j.1502-3931.2007.00091.x

Sutton, M.D., Garwood, R.J., Siveter, D.J., and Siveter, D.J. 2012. SPIERS and VAXML: A software toolkit for tomographic visualisation and a format for virtual specimen interchange. *Palaeontologia electronica*, 15.2.5T:1-14 palaeo-electronica.org/content/issue-2-2012-technical-articles/226-virtual-palaeontology-toolkit

Witmer, L.M. 1995. The extant phylogenetic bracket and the importance of reconstructing soft tissues in fossils, p. 19-33. In Thomason, J.J. (ed.), *Functional morphology in vertebrate paleontology*. Cambridge University Press, New York.

APPENDIX 1.

Element and specimen numbers for the reconstruction of *Panthera atrox*.

Specimen number	Element
LACMP23-555	Skull
LACMP23-4819	R dentary
LACMP23-3874	C1
LACMP23-3944	C2
LACMP23-3794	C3
LACMP23-1243	C4
LACMP23-3857	C5
LACMP23-1193	C6
LACMP23-4434	C7
LACMP23-666	T1 (T2 replicated)
LACMP23-666	T2
LACMP23-3719	T3
LACMP23-3764	T4
LACMP23-3764	T5 (T4 replicated)
LACMP23-3765	T6
LACMP23-3765	T7 (T6 replicated)
LACMP23-3754	T8
LACMP23-3715	T9
LACMP2458-19	T10 (“skeleton 2”)
LACMP23-3722	T11
LACMP23-9667	T12
LACMP23-3781	T13
LACMP23-3875	L1
LACMP23-3879	L2
LACMP23-3894	L3
LACMP23-3919	L4
LACMP23-4027	L5
LACMP23-3887	L6
LACMP23-3924	L7
LACMP23-3927	Sacrum
LACMP23-3700	Right scapula
LACMP23-1111	Left humerus
LACMP23-693	Left radius
LACMP23-3694	Left ulna
LACMP23-8741	Right innominate
LACMP23-918	Left femur
LACMP23-3696	Left tibia
NMS.Z.2015.128	Ribs, tail, manus, pes

APPENDIX 2.

Scaling equations for the forelimb muscles from Cuff et al. (2016a) and calculated muscle belly lengths for the mean, lower, and upper bounds of muscles for *Panthera atrox*. Serrat. vent. cerv. = m. serratus ventralis cervicus, Serrat. vent. thor. = m. serratus ventralis thoracis, Abd. dig. 1 = m. abductor digiti 1. Ext. = extensor, Flex. = flexor.

Muscle	Slope	Lower Limit	Upper Limit	Intercept	Mean	Lower	Upper
Latissimus dorsi	0.245	0.155	0.386	-0.757	0.646	0.400	1.374
Trapezius cervicis	0.447	0.168	1.19	-1.46	0.379	0.085	19.92
Trapezius thoracis	0.244	0.135	0.440	-1.13	0.275	0.154	0.783
Rhomboideus capitis	0.419	0.174	1.01	-1.34	0.428	0.116	9.804
Rhomboideus cervicis	0.340	0.147	0.782	-1.43	0.230	0.082	2.429
Rhomboideus thoracis	0.283	0.173	0.464	-1.35	0.204	0.113	0.538
Omotransversarius	0.250	0.201	0.312	-1.04	0.350	0.268	0.487
Cleidocephalicus	0.272	0.180	0.412	-1.02	0.405	0.248	0.853
Cleidobrachialis	0.299	0.238	0.376	-1.17	0.336	0.242	0.507
Serrat. Vent. Cerv.	0.244	0.186	0.321	-1.18	0.244	0.179	0.368
Serrat. Vent. Thor.	0.267	0.145	0.493	-1.24	0.240	0.125	0.801
Pectoralis superficialis	0.307	0.225	0.418	-1.14	0.372	0.241	0.674
Pectoralis profundus	0.395	0.236	0.663	-1.11	0.642	0.274	2.672
Supraspinatus	0.327	0.268	0.398	-1.22	0.344	0.252	0.505
Infraspinatus	0.265	0.194	0.363	-1.20	0.261	0.178	0.440
Deltoideus acromion	0.297	0.231	0.381	-1.42	0.184	0.130	0.289
Deltoideus spinous	0.267	0.245	0.292	-1.33	0.195	0.173	0.222
Teres major	0.286	0.232	0.353	-1.21	0.286	0.214	0.408
Subscapularis	0.279	0.213	0.365	-1.24	0.254	0.179	0.403
Teres minor	0.356	0.154	0.819	-1.87	0.091	0.031	1.076
Coracobrachialis	1.09	0.468	2.54	-2.72	0.644	0.023	1491
Triceps longus	0.417	0.173	1.005	-1.43	0.348	0.095	7.992
Triceps lateralis	0.249	0.198	0.313	-1.13	0.277	0.211	0.389
Triceps medius	0.277	0.199	0.385	-1.24	0.253	0.167	0.452
Triceps accessory	0.308	0.269	0.352	-1.26	0.281	0.229	0.357
Biceps brachi	0.259	0.214	0.315	-1.19	0.257	0.201	0.346
Brachialis	0.412	0.213	0.794	-1.48	0.297	0.103	2.279
Anconeus	0.301	0.225	0.404	-1.48	0.165	0.110	0.286
Ext. carpi radialis	0.305	0.224	0.415	-1.22	0.310	0.201	0.558
Ext. digitorum communis	0.296	0.134	0.653	-1.31	0.236	0.100	1.587
Ext. digitorum lateralis	0.575	0.270	1.23	-1.72	0.415	0.081	13.3
Ext. carpi ulnaris	0.287	0.195	0.423	-1.24	0.264	0.161	0.544
Flex. carpi ulnaris ulnar	0.264	0.162	0.432	-1.19	0.262	0.151	0.641
Flex. carpi ulnaris humeral	0.275	0.185	0.409	-1.17	0.295	0.182	0.604
Brachioradialis	1.37	0.676	2.77	-2.79	2.410	0.060	4289
Supinator	0.316	0.220	0.454	-1.57	0.147	0.088	0.307
Pronator teres	0.316	0.232	0.431	-1.40	0.216	0.138	0.398
Pronator quadratus	0.497	0.326	0.756	-1.75	0.254	0.102	1.014
Flex. carpi radialis	0.305	0.256	0.363	-1.29	0.259	0.199	0.353
Flex. digitorum complex	0.237	0.163	0.345	-1.10	0.284	0.191	0.505
Abd. Dig. 1	0.576	0.388	0.856	-1.71	0.418	0.153	1.859

APPENDIX 3.

Scaling equations for the forelimb muscles from Cuff et al. (2016a) and calculated tendon lengths for the mean, lower, and upper bounds of muscles for *Panthera atrox.* Abd. dig. 1 = m. abductor digiti 1. Ext. = extensor, Flex. = flexor.

Muscle	Slope	Lower Limit	Upper Limit	Intercept	Mean	Lower	Upper
Cleidobrachialis	0.945	0.433	2.06	-3.04	0.140	0.009	54.70
Supraspinatus	0.719	0.032	16.2	-3.01	0.045	0.001	$2.44x10^{34}$
Infraspinatus	1.18	0.751	1.84	-3.42	0.203	0.021	7.029
Deltoideus spinous	1.29	0.072	22.9	-3.92	0.113	0.000	$1.21x10^{49}$
Teres major	-0.687	-1.649	-0.286	-1.14	0.002	0.000	0.016
Subscapularis	0.350	0.199	0.614	-2.46	0.022	0.010	0.092
Triceps longus	0.727	0.420	1.26	-2.57	0.130	0.025	2.206
Triceps lateralis	1.03	0.387	2.77	-3.39	0.101	0.003	1029
Triceps medius	0.598	0.225	1.59	-2.25	0.136	0.019	26.37
Biceps brachi	0.289	0.168	0.497	-1.66	0.102	0.054	0.310
Brachialis	0.530	0.285	0.983	-2.46	0.059	0.016	0.658
Ext. carpi radialis	0.336	0.205	0.552	-1.57	0.163	0.081	0.515
Ext. digitorum communis	-0.661	-1.580	-0.276	-0.313	0.014	0.000	0.111
Ext. digitorum lateralis	0.242	0.123	0.475	-1.332	0.169	0.090	0.588
Ext. carpi ulnaris	0.289	0.134	0.624	-1.457	0.163	0.071	0.977
Flex. carpi ulnaris ulnar	-0.310	-0.823	-0.117	-0.964	0.021	0.001	0.058
Flex. carpi ulnaris humeral	0.534	0.111	2.575	-2.20	0.108	0.011	5765
Supinator	-1.37	-8.50	-0.222	0.503	0.002	0.000	0.974
Pronator quadratus	0.552	0.154	1.987	-2.41	0.073	0.009	154.6
Flex. carpi radialis	0.212	0.088	0.511	-1.58	0.081	0.042	0.399
Flex. digitorum complex	0.262	0.151	0.456	-1.36	0.177	0.098	0.496
Abd. Dig. 1	0.691	0.365	1.308	-2.25	0.223	0.039	6.010

APPENDIX 4.

Scaling equations for the forelimb muscles from Cuff et al. (2016a) and calculated muscle belly masses for the mean, lower,and upper bounds of muscles for *Panthera atrox*. Serrat. vent. cerv. = m. serratus ventralis cervicus, Serrat. vent. thor. = m. serratus ventralis thoracis, Abd. dig. 1 = m. abductor digiti 1. Ext. = extensor, Flex. = flexor.

Muscle	Slope	Lower Limit	Upper Limit	Intercept	Mean	Lower	Upper
Latissimus dorsi	1.12	0.993	1.26	-2.34	1.776	0.906	3.792
Trapezius cervicis	1.05	0.913	1.22	-3.08	0.229	0.108	0.543
Trapezius thoracis	1.07	0.867	1.32	-3.09	0.242	0.083	0.910
Rhomboideus capitis	1.27	0.877	1.84	-3.58	0.232	0.028	4.913
Rhomboideus cervicis	1.15	0.859	1.55	-3.02	0.444	0.093	3.618
Rhomboideus thoracis	1.07	0.734	1.57	-3.30	0.156	0.025	2.231
Omotransversarius	1.08	0.877	1.34	-3.28	0.169	0.056	0.656
Cleidocephalicus	1.18	0.874	1.58	-3.04	0.484	0.096	4.238
Cleidobrachialis	1.14	0.939	1.39	-2.94	0.509	0.171	1.915
Serrat. Vent. Cerv.	0.977	0.702	1.36	-2.55	0.523	0.121	4.027
Serrat. Vent. Thor.	0.949	0.779	1.16	-2.46	0.552	0.223	1.672
Pectoralis superficialis	1.22	0.917	1.63	-3.08	0.567	0.111	4.987
Pectoralis profundus	1.07	0.887	1.29	-2.20	1.923	0.720	6.290
Supraspinatus	1.02	0.844	1.23	-2.36	1.001	0.395	3.082
Infraspinatus	0.991	0.799	1.23	-2.45	0.699	0.251	2.491
Deltoideus acromion	1.04	0.881	1.24	-3.21	0.162	0.068	0.451
Deltoideus spinous	1.08	0.877	1.33	-3.22	0.190	0.064	0.725
Teres major	1.07	0.921	1.25	-2.74	0.554	0.246	1.429
Subscapularis	0.963	0.797	1.16	-2.41	0.670	0.276	1.959
Teres minor	0.982	0.796	1.21	-3.73	0.035	0.013	0.120
Coracobrachialis	1.55	0.734	3.26	-4.46	0.133	0.002	1233
Triceps longus	1.06	0.922	1.23	-2.27	1.562	0.732	3.744
Triceps lateralis	1.05	0.906	1.22	-2.67	0.582	0.270	1.417
Triceps medius	1.05	0.840	1.31	-3.14	0.197	0.064	0.804
Triceps accessory	0.968	0.758	1.23	-3.15	0.123	0.040	0.513
Biceps brachi	1.06	0.895	1.25	-2.73	0.531	0.223	1.485
Brachialis	1.00	0.652	1.54	-3.19	0.138	0.021	2.473
Anconeus	1.05	0.801	1.37	-3.57	0.072	0.019	0.404
Ext. carpi radialis	1.03	0.822	1.30	-3.09	0.201	0.065	0.828
Ext. digitorum communis	1.17	0.929	1.48	-3.45	0.186	0.051	0.945
Ext. digitorum lateralis	1.02	0.761	1.36	-3.63	0.054	0.014	0.300
Ext. carpi ulnaris	1.10	0.681	1.78	-3.66	0.077	0.008	2.868
Flex. carpi ulnaris ulnar	1.19	0.814	1.74	-3.61	0.139	0.019	2.628
Flex. carpi ulnaris humeral	1.10	0.933	1.30	-3.34	0.162	0.066	0.474
Brachioradialis	1.49	1.261	1.75	-4.11	0.218	0.065	0.900
Supinator	1.02	0.747	1.40	-3.77	0.039	0.009	0.292
Pronator teres	1.03	0.836	1.28	-3.29	0.128	0.044	0.476
Pronator quadratus	1.22	0.925	1.61	-3.98	0.071	0.015	0.574
Flex. carpi radialis	0.929	0.792	1.09	-3.39	0.058	0.028	0.138
Flex. digitorum complex	0.998	0.877	1.13	-2.61	0.499	0.262	1.038
Abd. Dig. 1	0.861	0.566	1.31	-3.41	0.039	0.008	0.425

APPENDIX 5.

Scaling equations for the forelimb muscles from Cuff et al. (2016a) and calculated tendon masses for the mean, lower, and upper bounds of muscles for *Panthera atrox.* Abd. dig. 1 = m. abductor digiti 1, Ext. = extensor, Flex. = flexor.

Muscle	Slope	Lower Limit	Upper Limit	Intercept	Mean	Lower	Upper
Cleidobrachialis	-2.71	-9.826	-0.748	0.836	0.000	0.000	0.127
Supraspinatus	0.651	0.087	4.88	-4.39	0.001	0.000	8.38×10^{6}
Infraspinatus	1.289	0.636	2.61	-4.40	0.038	0.001	44.46
Deltoideus spinous	-0.349	-5.351	-0.023	-2.54	0.000	0.000	0.003
Teres major	0.621	0.376	1.027	-4.41	0.001	0.000	0.009
Triceps longus	0.852	0.431	1.68	-4.22	0.006	0.001	0.470
Triceps lateralis	1.02	0.627	1.65	-4.65	0.005	0.001	0.154
Triceps medius	1.70	0.772	3.75	-5.94	0.010	0.000	548.4
Biceps brachi	0.933	0.748	1.16	-4.10	0.012	0.004	0.040
Brachialis	0.943	0.495	1.80	-4.71	0.003	0.000	0.287
Ext. carpi radialis	0.915	0.765	1.09	-4.24	0.008	0.003	0.019
Ext. digitorum communis	1.44	0.970	2.12	-4.46	0.074	0.006	2.906
Ext. digitorum lateralis	0.958	0.722	1.27	-4.32	0.008	0.002	0.042
Ext. carpi ulnaris	0.833	0.455	1.52	-4.23	0.005	0.001	0.199
Flex. carpi ulnaris ulnar	1.16	0.743	1.82	-5.21	0.003	0.000	0.101
Flex. carpi ulnaris humeral	0.984	0.643	1.51	-5.08	0.002	0.000	0.026
Supinator	1.57	0.251	9.79	-6.08	0.004	0.000	4.09×10^{6}
Pronator quadratus	0.953	0.310	2.93	-4.58	0.004	0.000	162.0
Flex. carpi radialis	0.660	0.450	0.967	-4.28	0.002	0.001	0.009
Flex. digitorum complex	0.943	0.692	1.29	-3.24	0.087	0.023	0.541
Abd. Dig. 1	0.730	0.403	1.32	-4.24	0.003	0.000	0.066

APPENDIX 6.

Scaling equations for the hindlimb muscles from Cuff et al. (2016b) and calculated muscle belly lengths for the mean, lower, and upper bounds of muscles for *Panthera atrox*. Gastroc. = gastrocnemius, dig. = digitorum, supefic. = superficialis.

Muscle	Slope	Lower LimitLower Limit	Upper Limit	Intercept	Mean	Lower	Upper
Biceps femoris	0.264	0.172	0.406	-0.988	0.420	0.257	0.895
Caudofemoralis	0.281	0.185	0.426	-1.079	0.373	0.223	0.811
Sartorius	0.327	0.258	0.414	-0.941	0.654	0.453	1.040
Tensor fascia latae	0.292	0.221	0.387	-1.398	0.190	0.130	0.315
Vastus lateralis	0.286	0.232	0.352	-1.072	0.389	0.293	0.553
Rectus femoris	0.366	0.204	0.658	-1.227	0.419	0.176	1.984
Vastus medius	0.268	0.210	0.342	-1.077	0.350	0.257	0.519
Vastus intermedius	0.554	0.264	1.164	-1.597	0.486	0.103	12.60
Semitendinosus	0.279	0.242	0.322	-0.980	0.464	0.381	0.583
Semimembranosus	0.564	0.270	1.178	-1.451	0.718	0.150	18.95
Gracilis	0.244	0.132	0.449	-1.155	0.257	0.142	0.770
Gluteus superficialis	0.321	0.213	0.484	-1.479	0.184	0.103	0.439
Gluteus medius	0.345	0.290	0.412	-1.405	0.249	0.185	0.354
Gluteus profundus	0.353	0.255	0.489	-1.454	0.231	0.137	0.476
Piriformis	0.167	0.101	0.276	-1.432	0.090	0.063	0.162
Gemelli	0.380	0.188	0.769	-1.693	0.154	0.055	1.226
Quadratus femoris	0.301	0.228	0.396	-1.600	0.125	0.085	0.208
Obturator externus	0.330	0.271	0.402	-1.671	0.124	0.091	0.182
Obturator internus	0.288	0.172	0.480	-1.595	0.118	0.064	0.329
Pectineus	0.455	0.234	0.883	-1.626	0.268	0.083	2.625
Adductor magnus	0.305	0.198	0.471	-1.114	0.392	0.221	0.900
Adductor brevis	0.310	0.175	0.551	-1.388	0.214	0.104	0.773
Iliacus	1.388	0.090	21.318	-3.465	0.564	0.001	$8.35x10^4$
Psoas major	0.384	0.256	0.575	-1.142	0.558	0.283	1.547
Psoas minor	0.318	0.201	0.504	-1.165	0.373	0.200	1.004
Gastroc. lateralis	0.327	0.219	0.490	-1.235	0.334	0.187	0.796
Gastroc. medius	0.262	0.216	0.317	-1.142	0.291	0.228	0.392
Superfic. dig. flexor	0.264	0.131	0.530	-1.144	0.293	0.145	1.211
Soleus	0.212	0.147	0.304	-1.061	0.268	0.191	0.439
Dig. extensor longus	0.265	0.150	0.468	-1.150	0.291	0.157	0.859
Tibialis cranialis	0.237	0.130	0.432	-1.095	0.284	0.160	0.800
Popliteus	0.375	0.266	0.530	-1.594	0.189	0.105	0.432
Dig. extensor lateralis	0.265	0.196	0.359	-1.282	0.215	0.149	0.354
Peroneus longus	0.236	0.145	0.383	-1.201	0.222	0.137	0.486
Peroneus brevis	0.192	0.112	0.330	-1.144	0.200	0.130	0.400
Deep digital flexor medial	0.307	0.196	0.480	-1.236	0.298	0.165	0.751
Deep digital flexor lateral	0.406	0.171	0.965	-1.430	0.324	0.092	6.383
Tibialis caudalis	0.413	0.256	0.666	-1.522	0.272	0.118	1.046

APPENDIX 7.

Scaling equations for the hindlimb muscles from Cuff et al. (2016b) and calculated tendon lengths for the mean, lower, and upper bounds of muscles for *Panthera atrox*. Gastroc. = gastrocnemius, Dig. = digitorum, Supefic. = superficialis.

Muscle	Slope	Lower Limit	Upper Limit	Intercept	Mean	Lower	Upper
Caudofemoralis	0.496	0.304	0.812	-1.612	0.345	0.123	1.854
Tensor fascia latae	0.330	0.160	0.679	-1.298	0.293	0.119	1.880
Rectus femoris	1.307	0.099	17.288	-3.216	0.650	0.001	6.86×10^{3}
Vastus medius	0.264	0.144	0.483	-2.155	0.029	0.015	0.092
Vastus intermedius	-0.875	-20.805	-0.037	-0.659	0.002	0.000	0.180
Semitendinosus	0.440	0.230	0.841	-1.893	0.134	0.044	1.138
Semimembranosus	0.467	0.162	1.348	-2.446	0.043	0.008	4.746
Gracilis	0.558	0.093	3.355	-2.349	0.088	0.007	2.65×10^{5}
Gluteus profundus	-0.604	-3.758	-0.097	-0.893	0.005	0.000	0.076
Piriformis	0.278	0.015	5.158	-2.279	0.023	0.006	4.69×10^{9}
Obturator internus	0.353	0.068	1.842	-1.924	0.078	0.017	220.4
Psoas major	0.074	0.003	1.689	-1.407	0.058	0.040	320.7
Psoas minor	0.182	0.035	0.937	-1.563	0.072	0.033	4.059
Gastroc. lateralis	0.208	0.102	0.424	-1.624	0.072	0.041	0.228
Gastroc. medius	0.470	0.235	0.939	-1.952	0.137	0.039	1.677
Superfic. dig. flexor	0.887	0.369	2.134	-2.483	0.373	0.023	289.5
Soleus	0.058	0.002	1.424	-1.749	0.024	0.018	35.43
Dig. extensor longus	0.445	0.188	1.051	-1.601	0.269	0.068	6.825
Tibialis cranialis	0.366	0.183	0.731	-1.803	0.111	0.042	0.777
Popliteus	0.564	0.075	4.223	-2.329	0.095	0.007	2.85×10^{7}
Dig. extensor lateralis	0.427	0.245	0.745	-1.484	0.320	0.121	1.747
Peroneus longus	0.331	0.148	0.738	-1.546	0.166	0.063	1.456
Peroneus brevis	0.648	0.239	1.753	-2.117	0.242	0.027	87.82
Deep digital flexor medial	0.336	0.148	0.760	-1.302	0.299	0.110	2.877
Deep digital flexor lateral	0.525	0.272	1.015	-1.550	0.465	0.120	6.322
Tibialis caudalis	0.313	0.132	0.740	-1.469	0.180	0.069	1.759

APPENDIX 8.

Scaling equations for the hindlimb muscles from Cuff et al. (2016b) and calculated muscle belly masses for the mean, lower, and upper bounds of muscles for *Panthera atrox*. Gastroc. = gastrocnemius, Dig. = digitorum, Supefic. = superficialis.

Muscle	Slope	Lower Limit	Upper Limit	Intercept	Mean	Lower	Upper
Biceps femoris	0.998	0.862	1.155	-2.124	1.537	0.745	3.553
Caudofemoralis	1.353	0.950	1.928	-3.423	0.515	0.060	11.03
Sartorius	1.090	0.956	1.242	-2.636	0.775	0.380	1.745
Tensor fascia latae	1.240	0.976	1.575	-3.138	0.542	0.133	3.236
Vastus lateralis	0.955	0.788	1.156	-2.228	0.962	0.396	2.815
Rectus femoris	0.964	0.841	1.103	-2.391	0.693	0.361	1.462
Vastus medius	0.924	0.732	1.165	-2.452	0.487	0.175	1.769
Vastus intermedius	0.796	0.650	0.976	-2.619	0.168	0.077	0.439
Semitendinosus	1.093	0.929	1.286	-2.697	0.684	0.285	1.915
Semimembranosus	1.061	0.789	1.428	-2.322	1.369	0.320	9.683
Gracilis	1.213	0.767	1.917	-3.082	0.534	0.050	22.90
Gluteus superficialis	1.053	0.832	1.334	-3.257	0.153	0.047	0.681
Gluteus medius	1.220	1.120	1.330	-2.800	1.063	0.622	1.905
Gluteus profundus	0.906	0.743	1.106	-3.147	0.090	0.037	0.261
Piriformis	0.828	0.630	1.087	-2.948	0.093	0.033	0.372
Gemelli	1.155	0.827	1.612	-3.510	0.146	0.025	1.675
Quadratus femoris	0.785	0.556	1.109	-3.160	0.046	0.013	0.256
Obturator externus	1.085	0.909	1.295	-3.288	0.168	0.066	0.516
Obturator internus	1.063	0.784	1.441	-3.214	0.178	0.040	1.331
Pectineus	0.903	0.635	1.285	-3.124	0.093	0.022	0.711
Adductor magnus	1.056	0.729	1.530	-2.374	1.181	0.206	14.8
Adductor brevis	0.878	0.547	1.409	-2.710	0.211	0.036	3.574
Iliacus	2.272	0.456	11.327	-5.532	0.538	0.000	$5.12x10^2$
Psoas major	1.172	0.849	1.619	-2.821	0.785	0.140	8.520
Psoas minor	1.098	0.801	1.505	-3.159	0.242	0.050	2.131
Gastroc. lateralis	0.923	0.721	1.181	-2.562	0.377	0.129	1.496
Gastroc. medius	0.874	0.737	1.036	-2.545	0.302	0.146	0.718
Superfic. dig. flexor	0.842	0.623	1.138	-2.876	0.119	0.037	0.575
Soleus	0.850	0.669	1.080	-2.880	0.123	0.047	0.419
Dig. extensor longus	0.902	0.527	1.544	-3.166	0.084	0.011	2.577
Tibialis cranialis	1.025	0.725	1.449	-3.046	0.213	0.043	2.00
Popliteus	0.846	0.683	1.048	-3.225	0.054	0.023	0.159
Dig. extensor lateralis	0.835	0.522	1.336	-3.518	0.026	0.005	0.378
Peroneus longus	1.324	0.768	2.283	-3.800	0.185	0.010	30.82
Peroneus brevis	0.912	0.600	1.387	-3.496	0.041	0.008	0.500
Deep digital flexor medial	1.038	0.726	1.485	-3.188	0.165	0.031	1.788
Deep digital flexor lateral	1.017	0.630	1.643	-3.220	0.137	0.017	3.865
Tibialis caudalis	1.263	0.961	1.660	-3.856	0.117	0.023	0.975

APPENDIX 9.

Scaling equations for the hindlimb muscles from Cuff et al. (2016b) and calculated tendon masses for the mean, lower, and upper bounds of muscles for *Panthera atrox*. Gastroc. = gastrocnemius, Dig. = digitorum, Supefic. = superficialis.

Muscle	Slope	Lower Limit	Upper Limit	Intercept	Mean	Lower	Upper
Caudofemoralis	1.190	0.455	3.111	-4.484	0.019	0.000	527.3
Tensor fascia latae	0.964	0.690	1.347	-3.599	0.043	0.010	0.333
Rectus femoris	1.441	0.059	35.233	-4.439	0.079	0.000	$1.53x10^{77}$
Vastus medius	1.029	0.621	1.704	-4.782	0.004	0.000	0.147
Vastus intermedius	-0.488	-11.839	-0.020	-2.481	0.000	0.000	0.003
Semitendinosus	0.962	0.607	1.525	-4.575	0.005	0.001	0.091
Semimembranosus	0.750	0.419	1.342	-4.321	0.003	0.000	0.061
Gracilis	1.225	0.445	3.372	-4.638	0.016	0.000	1492
Gluteus profundus	0.574	0.176	1.876	-4.360	0.001	0.000	0.971
Piriformis	0.893	0.229	3.492	-4.675	0.002	0.000	2602
Obturator internus	1.035	0.127	8.421	-4.487	0.008	0.000	$1.05x10^{15}$
Psoas major	1.725	1.080	2.756	-5.129	0.074	0.002	18.08
Psoas minor	0.756	0.212	2.692	-4.446	0.002	0.000	61.68
Gastroc. lateralis	1.014	0.642	1.601	-4.036	0.021	0.003	0.471
Gastroc. medius	0.973	0.547	1.729	-3.929	0.021	0.002	1.19
Superfic. dig. flexor	1.710	1.153	2.536	-4.468	0.311	0.016	25.49
Soleus	0.770	0.052	11.341	-4.509	0.002	0.000	$5.82x10^{21}$
Dig. extensor longus	1.568	1.063	2.313	-4.610	0.105	0.007	5.61
Tibialis cranialis	1.010	0.666	1.532	-4.696	0.004	0.001	0.071
Popliteus	0.814	0.423	1.566	-4.388	0.003	0.000	0.174
Dig. extensor lateralis	0.829	0.595	1.155	-4.389	0.003	0.001	0.019
Peroneus longus	1.856	0.726	4.745	-5.506	0.062	0.000	$3.06x10^{5}$
Peroneus brevis	0.950	0.553	1.633	-4.589	0.004	0.000	0.156
Deep digital flexor medial	1.335	0.711	2.508	-4.300	0.062	0.002	32.40
Deep digital flexor lateral	1.035	0.659	1.625	-3.791	0.040	0.005	0.940
Tibialis caudalis	1.129	0.630	2.023	-4.585	0.011	0.001	1.266

APPENDIX 10.

Scaling equations for the vertebral muscles from Cuff et al. (2016a, 2016b) and calculated muscle belly lengths for the mean, lower, and upper bounds of muscles for *Panthera atrox.* Longis. = longissimus, Iliocost. = iliocostalis, Multifid. = multifidus.

Muscle	Slope	Lower Limit	Upper Limit	Intercept	Mean	Lower	Upper
Rectus capitis	0.208	0.080	0.541	-1.43	0.112	0.057	0.662
Splenius cervicis	0.234	0.174	0.316	-0.946	0.395	0.286	0.610
Serratus dorsalis cranialis	0.239	0.079	0.719	-1.45	0.127	0.054	1.647
Serratus dorsalis caudalis	0.186	0.070	0.496	-1.50	0.085	0.046	0.444
Semispinalis capitis biventer	1.36	0.683	2.71	-2.55	4.009	0.108	5326
Semispinalis capitis complexus	0.336	0.162	0.700	-1.11	0.470	0.185	3.267
Spinalis cervicis	0.240	0.098	0.591	-1.06	0.314	0.147	2.040
Spinalis thoracis	0.309	0.252	0.380	-0.910	0.641	0.472	0.934
Longissimus capitis	0.287	0.130	0.633	-1.16	0.323	0.140	2.044
Longissimus cervicis	0.227	0.121	0.425	-0.920	0.405	0.230	1.163
Longissimus thoracis	0.340	0.208	0.556	-0.872	0.827	0.409	2.612
Iliocostalis thoracis	0.266	0.183	0.386	-0.809	0.640	0.412	1.215
Multifidis throacis	0.305	0.213	0.435	-0.852	0.713	0.439	1.429
Longis. lumborum	0.603	0.197	1.849	-1.403	0.987	0.113	758.5
Iliocost. lumborum	0.358	0.216	0.594	-1.030	0.630	0.295	2.217
Multifid. lumborum	0.319	0.166	0.613	-0.919	0.661	0.293	3.165

APPENDIX 11.

Scaling equations for the vertebral muscles from Cuff et al. (2016a, 2016b) and calculated tendon lengths for the mean, lower, and upper bounds of muscles for *Panthera atrox.*

Muscle	Slope	Lower Limit	Upper Limit	Intercept	Mean	Lower	Upper
Serratus dorsalis cranialis	1.35	0.217	8.42	-3.772	0.228	0.001	5.43×10^{5}
Serratus dorsalis caudalis	-1.53	-6.001	-0.389	0.484	0.001	0.000	0.382

APPENDIX 12.

Scaling equations for the vertebral muscles from Cuff et al. (2016a, 2016b) and calculated muscle belly masses for the mean, lower, and upper bounds of muscles for *Panthera atrox.*

Muscle	Slope	Lower Limit	Upper Limit	Intercept	Mean	Lower	Upper
Rectus capitis	0.679	0.472	0.977	-2.58	0.098	0.032	0.480
Splenius cervicis	1.04	0.785	1.39	-2.86	0.366	0.092	2.31
Serratus dorsalis cranialis	1.00	0.523	1.93	-3.23	0.124	0.009	17.1
Serratus dorsalis caudalis	0.893	0.701	1.14	-3.17	0.080	0.029	0.294
Semispinalis capitis biventer	1.05	0.899	1.24	-2.93	0.325	0.143	0.9
Semispinalis capitis complexus	1.13	0.854	1.51	-3.12	0.325	0.073	2.38
Spinalis cervicis	0.992	0.532	1.85	-2.77	0.336	0.029	32.4
Spinalis thoracis	1.26	0.941	1.69	-2.98	0.877	0.160	8.52
Longissimus capitis	0.867	0.488	1.54	-3.21	0.064	0.008	2.32
Longissimus cervicis	0.673	0.338	1.34	-2.40	0.143	0.024	4.98
Longissimus thoracis	0.821	0.542	1.24	-1.94	0.916	0.207	8.76
Iliocostalis thoracis	0.899	0.743	1.09	-2.79	0.195	0.085	0.533
Multifidis throacis	0.893	0.784	1.02	-2.52	0.355	0.198	0.690
Longis. lumborum	1.26	0.652	2.43	-2.55	2.34	0.092	1230
Iliocost. lumborum	1.19	0.860	1.65	-2.58	1.49	0.258	17.0
Multifid. lumborum	0.942	0.705	1.26	-2.60	0.381	0.108	2.05

APPENDIX 13.

Scaling equations for the vertebral muscles from Cuff et al. (2016a, 2016b) and calculated tendon masses for the mean, lower, and upper bounds of muscles for *Panthera atrox*. Longis. = longissimus, Iliocost. = iliocostalis, Multifid. = multifidus.

Muscle	Slope	Lower Limit	Upper Limit	Intercept	Mean	Lower	Upper
Serratus dorsalis cranialis	1.36	0.609	3.03	-4.63	0.033	0.001	247.5
Serratus dorsalis caudalis	1.40	0.639	3.06	-4.94	0.020	0.000	141.3